Tetrahedral chalcopyrite quantum dots for solar-cell applications

Juho Ojajärvi,[1] Esa Räsänen,[1,a)] Sascha Sadewasser,[2] Sebastian Lehmann,[2,3] Philipp Wagner,[2,4] and Martha Ch. Lux-Steiner[2]
[1]*Nanoscience Center, Department of Physics, University of Jyväskylä, Jyväskylä FI-40014, Finland*
[2]*Helmholtz-Zentrum Berlin für Materialien und Energie, Hahn-Meitner-Platz 1, Berlin 14109, Germany*
[3]*Solid State Physics, Lund University, Box 118, Lund 22100, Sweden*
[4]*Institut des Matériaux Jean Rouxel, Université de Nantes, CNRS UMR 6502, Nantes 44322, France*

(Received 10 August 2011; accepted 28 August 2011; published online 15 September 2011)

Chalcopyrite structures are candidates for efficient intermediate-band solar cells in thin-film technology. Here, we examine a material combination of $CuInSe_2$ dots embedded in $CuGaS_2$ matrix and show that epitaxial growth leads to distinctive tetrahedral nanostructures. Our model calculations provide us with the optimal nanodot size to reach the maximum efficiency—in principle up to 61%. The optimal quantum dot satisfies the known physical constraints, and it is in excellent qualitative agreement with our grown samples. © *2011 American Institute of Physics*. [doi:10.1063/1.3640225]

Solar-cell technology is likely to have a remarkable impact on the society as long as we are able to develop more efficient and affordable solutions.[1] In addition to experiments on different materials and their combinations, realistic quantum simulations are indispensable in the progress.

On the conceptual and prototype level, the development of solar cells has gradually led to the so-called third generation with, e.g., dye-sensitized, hot-carrier, multijunction, and intermediate-band (IB) solar cells (IBSCs). As originally proposed by Luque and Martí[2] in 1997, the IB enhances the photogenerated current via a two-step absorption of sub-band-gap photons. The IB can be obtained by several means, e.g., by lone-pair bands, low-dimensional superlattices, or impurities. In any case, the IBSC has an impressive maximum efficiency of 63% for a *single* material. An experimental demonstration of the photocurrent created through the IB followed in 2006 (Ref. 3), and the first actual IBSC was created in 2009 (Ref. 4).

Chalcopyrite materials lead the current efficiency ranking of solar cells based on thin-film technologies.[5] The practical problem in using chalcopyrite structures in IBSC implementation is the difficulty in finding a suitable semiconductor matrix that has larger band gap than the nanostructured material. Very recently, however, significant progress has been made, and different Cu-containing materials such as $CuGaSe_2$ and $CuInSe_2$ have been proposed as an appropriate material combination.[6] Signals of electronic confinement have been observed, but the eventual applicability is largely dependent on the magnitude of interdiffusion phenomena and native defects in these materials.

The controllability of quantization could be improved by embedding a quantum-dot (QD) superlattice (with a small band gap) in a chalcopyrite matrix (larger gap).[7] In the QD superlattice, the offsets of the conduction (electrons) or the valence (holes) band, together with the quantum confinement provided by the QDs, give rise to a region that has a finite density of states in the matrix band gap. An approximation for the *minimum* QD diameter, ensuring at least one bound state, is given by $D_{\min} = \pi\hbar/\sqrt{2m^*\Delta E_b}$, where m^* is the effective mass of the charge carrier and ΔE_b is the energy barrier between the dot and the matrix, i.e., the conduction band offset (electrons) or the valence band offset (holes).[8] The *maximum* QD size can be estimated from the requirement that the thermal population of the excited states remains small.[9] Requiring less than 5%, occupation at room temperature (300 K) implies a level separation $kT \leq |E_1 - E_0|/3$, where E_0 and E_1 are the first two energy levels of the QD. For example, assuming a harmonic confinement for the charge carriers in three dimensions (see below), we have $E_1 - E_0 = 2E_0/3 = 2\hbar\omega/3$, where ω can be deduced from the size of the QD. It should be noted, however, that the thermal energy does not determine carrier recombination that is the ultimate limiting factor for the solar cell performance.

Here, we focus on a material combination of a $CuGaS_2$ matrix and $CuInSe_2$ QDs. The band alignments of this combination are shown in Fig. 1. The QD well depth is $V_0 = 1.18$ eV for electrons in the system, corresponding to the conduction-band offset. We note that in lack of direct experimental information about the band alignment in the $CuGaS_2/CuInSe_2$ heterojunction, we approximate it with the transitivity rule via $CuGaSe_2$ (green block in Fig. 1). The values have been taken from Ref. 10 supported by recent studies.[11,12] The validity of this approximation will be verified in future measurements; here, we only point out that the lattice constant of $CuGaS_2$ is 8% smaller than that of $CuInSe_2$, which might have a notable effect on the band alignment in the heterojunction. The effective mass of an

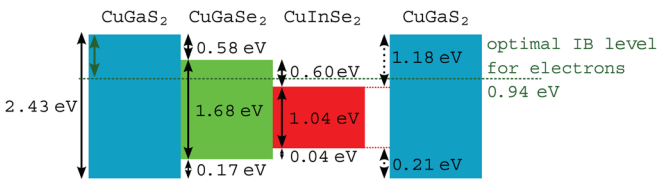

FIG. 1. (Color online) Band offsets for a combination of a $CuGaS_2$ matrix and $CuInSe_2$ dots at 0 K. In lack of direct experimental information, the $CuGaS_2/CuInSe_2$ heterojunction is approximated by the transitivity rule via $CuGaSe_2$.

a)Electronic mail: erasanen@jyu.fi.

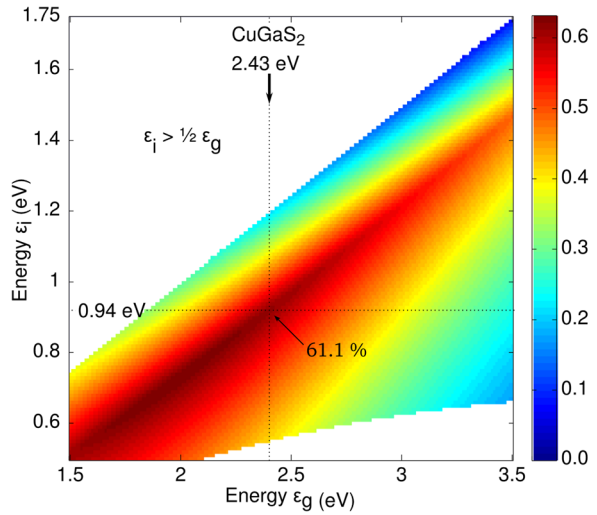

FIG. 2. (Color online) Efficiency of an intermediate-band solar cell[2] as a function of the embedding matrix band gap ϵ_g and the intermediate-band position ϵ_i. The dashed lines denote the $CuGaS_2$ matrix material considered in this work.

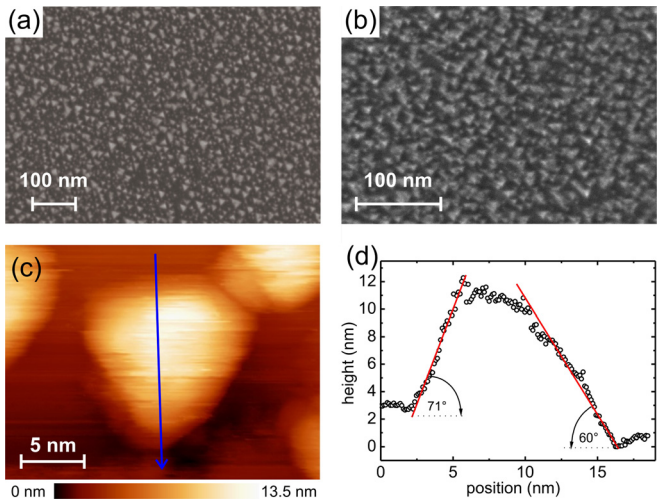

FIG. 3. (Color online) (a) SEM image of $CuInSe_2$ nanodots on Si(111) substrate grown by metal-organic vapor phase epitaxy. (b) SEM image of $CuGaSe_2$ nanodots grown by molecular beam epitaxy on a Si(111) substrate. (c) SEM image of one individual $CuGaSe_2$ nanodot. (d) Height profile of the $CuGaSe_2$ nanodot including the topography and the angles of the side and facets.

electron in $CuInSe_2$ is $m^* = 0.09\ m_0$, whereas in the matrix material $CuGaS_2$, the value is $m^* = 0.12\ m_0$ (Ref. 13).

Figure 2 shows the calculated IBSC efficiency (for concentrated sunlight) as a function of the band gap ϵ_g and the IB position ϵ_i. The position can be situated either from the valence or the conduction band; here, the latter option is used (see Fig. 1). In the calculation, we have directly applied the procedure of Luque and Martí.[2] The dashed vertical line corresponds to the IBSC implemented in $CuGaS_2$ with $\epsilon_g = 2.43$ eV. Correspondingly, the IB should be located at $\epsilon_i = 0.94$ eV (dashed horizontal line) for the maximum efficiency, which is as high as 61.1%. This is close to the *overall* IBSC maximum of 63.2% (Ref. 2).

We use molecular beam epitaxy to grow $CuGaSe_2$ samples on a Si(111) substrate. Furthermore, we also used metal-organic vapor phase epitaxy (MOVPE) for the growth of $CuInSe_2$ samples also on the same substrate. The growth of $CuInSe_2$ and $CuGaSe_2$, respectively, on Si(111) results in distinctive tetrahedral nanoclusters, as can be seen in the scanning electron microscopy (SEM) overview images in Figs. 3(a) and 3(b). Using scanning tunneling microscopy (STM), the three-dimensional surface topography was obtained, as shown by a close-up image of one $CuGaSe_2$ dot in Fig. 3(c). Using line profiles [Fig. 3(d)], the exact geometry can be analyzed, yielding the dot size and angles between the facets. A careful statistical evaluation of many dots[14] shows that the size of the tunneling tip has to be considered, as the measured geometry represents a convolution of the tip and the sample topography. Taking this into account, the dot diameter can be estimated to be between 2 and 20 nm for a variety of dots. The observed shape is close to an ideal tetrahedron and corresponds to the energetically most favorable configuration for chalcopyrites on a Si(111) substrate under these growth conditions.

Next, we focus on theoretical modeling of the obtained samples. We apply the effective mass approximation by assuming that the electrons are near the band minimum that can be approximated as parabolic. We use the effective mass of the $CuInSe_2$ QD which is $m^* = 0.09\ m_0$. We also assume that the electronic wave functions do not penetrate deep into the matrix material. Thus, we may use the same dielectric constant throughout the system (QD and the matrix material) which is here $\epsilon = 15.1$ (Ref. 15).

Besides using the effective mass approximation, we construct a model potential for the electronic confinement for the QD. In the literature, the external potential of semiconductor QDs has been most commonly approximated as harmonic, which is a valid model for various systems.[16,17] Here, however, we can explicitly use the experimental, *tetrahedral* structure shown in Fig. 3. Our model potential is now of the form $V_{\text{ext}}(\mathbf{r}) = -V_0 \exp[-(\mathbf{r}\cdot\mathbf{n}_i)^2/2L^2]$, where $\mathbf{n}_i$ are the normal vectors of the faces of the tetrahedron and L is the radius of the QD, or, more explicitly, it is the radius of the sphere fitting inside the tetrahedron as visualized in the inset of Fig. 4. Thus, the radius of the typical sample dot shown in Figs. 3(c)

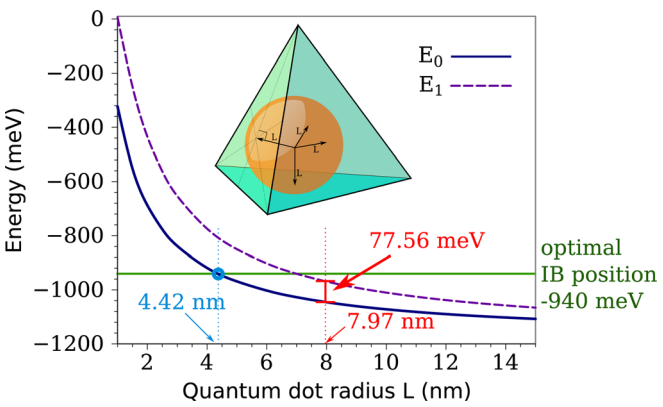

FIG. 4. (Color online) Energies of the first and second electronic states of a $CuInSe_2$ dot in a $CuGaS_2$ matrix as a function of the quantum dot radius. The solid horizontal line marks the optimal intermediate-band position corresponding to the radius of 4.42 nm (left dotted line). The right dotted line marks the maximum size of the quantum dot to satisfy the thermal constraint (see text). The bound-state constraint corresponds the left border of the figure (~1 nm). Inset: Tetrahedral model potential used in the calculations. The distance L is the radius of the sphere fitting inside the tetrahedron.

and 3(d) is approximately $L_{exp} = 3\ldots4$ nm. The depth of the potential $V_0 = 1.18$ eV is set to be equal to the valence band offset between the dot and the matrix materials (see Fig. 1). The Gaussian form of V_{ext} enables us to model the slowly varying confinement resulting from the smooth interface between the QD and matrix regions. On the other hand, in the vicinity of the QD center, the potential is close to harmonic, which can be regarded as a valid approximation with respect to previous QD studies.[16,17] We use the OCTOPUS code[18] for solving the single-particle Schrödinger equation in the model potential.

To determine the optimal size L of the tetrahedral QD in our model, we compute the lowest single-electron eigenenergies as a function of L. The energies are then compared, on one hand, to the optimal IB position and, on the other hand, to the bound-state and thermal conditions given above. The results for the two lowest levels are given in Fig. 4 (higher levels omitted). First, the optimal IB position can be clearly attained in the $CuInSe_2/CuGaS_2$ material combination—note that this is not an obvious property due to strong dependencies of the energy levels and IB positions on the material parameters, respectively. The optimal radius, i.e., the one yielding the highest efficiency according to Fig. 2, is $L_{opt} = 4.42$ nm.

The smallest QD size satisfying the constraint for having at least one bound state is found to be $L_{min} = 0.94$ nm. Then, the largest QD size still satisfying the thermal constraint is $L_{max} = 7.97$ nm. Interestingly, the grown samples shown in Fig. 3 have a size range that matches well with these theoretical constraints. Moreover, the most typical QDs—as the one shown in Figs. 3(c) and 3(d)—have $L_{exp} = 3\ldots4$ nm (see the definition of L above), which is in a qualitative agreement with the highest theoretical efficiency obtained at $L_{opt} = 4.42$ nm. Thus, according to our analysis, the use of $CuInSe_2$ QDs embedded in a $CuGaS_2$ matrix as IBSCs seems feasible. However, application of QDs in an IBSC requires *controlled* growth of periodic tetrahedral structures regarding their size, shape, and structuring. This is the fundamental aim of the future efforts, and we hope that the proof of concept demonstrated in this work motivates more studies.

To summarize, we have analyzed, both theoretically and experimentally, the usefulness of tetrahedral chalcopyrite quantum dots in intermediate-band solar cell applications. We have shown that the material combination under consideration, i.e., a $CuGaS_2$ matrix and $CuInSe_2$ dots, yields an impressive theoretical maximum efficiency of 61%. Our experiments based on molecular beam epitaxy and metal-organic vapor phase epitaxy clearly reveal the tetrahedral shape of both $CuInSe_2$ and $CuGaSe_2$ nanostructures. We have constructed a realistic model for the single-dot system and shown that the dot size that yields the optimal efficiency is in qualitative agreement with the experimental samples. Moreover, the important condition for the existence of a bound state as well as the thermal condition for the level population are satisfied. Overall, we hope that the present study serves as an elemental guideline to map the individual chalcopyrite quantum-dot properties to intermediate-band solar cells of technological relevance.

We thank David Fuertes Marrón for useful discussions and CSC—Finnish IT Center for Science—for the CPU time. This work has been supported by the Fortum Foundation and the Academy of Finland.

[1]E. Cartlidge, Phys. World **20**, 20 (2007).
[2]A. Luque and A. Martí, Phys. Rev. Lett. **78**, 5014 (1997).
[3]A. Martí, E. Antolín, C. R. Stanley, C. D. Farmer, N. López, P. Díaz, E. Cánovas, P. G. Linares, and A. Luque, Phys. Rev. Lett. **97**, 247701 (2006).
[4]W. Wang, A. S. Lin, and J. D. Phillips, App. Phys. Lett. **95**, 011103 (2009).
[5]M. A. Green, K. Emery, Y. Hishikawa, and W. Warta, Prog. Photovoltaics **19**, 84 (2011).
[6]D. F. Marrón, E. Cánovas, M. Y. Levy, A. Martí, A. Luque, M. Afshar, J. Albert, S. Lehmann, D. Abou-Ras, S. Sadewasser, and N. Barreau, Sol. Energy Mater. Sol. Cells **94**, 1912 (2010).
[7]A. Martí, L. Cuadra, and A. Luque, Physica E **14**, 150 (2002).
[8]D. Bimberg, M. Grundmann, and N. N. Ledentsov, *Quantum Dot Heterostructures* (John, UK, 1998).
[9]D. F. Marrón, A. Martí, and A. Luque, Phys. Status Solidi A **206**, 1021 (2009).
[10]S.-H. Wei and A. Zunger, J. Appl. Phys. **78**, 3846 (1995).
[11]S. Chen, X. G. Gong, and S.-H. Wei, Phys. Rev. B **75**, 205209 (2007).
[12]S. Chen, A. Walsh, J.-H. Yang, X. G. Gong, L. Sun, P.-X. Yang, J.-H. Chu, and S.-H. Wei, Phys. Rev. B **83**, 125201 (2011).
[13]S. Lankes, M. Meier, T. Reisinger, and W. Gebhardt, J. App. Phys. **80**, 4049 (1996).
[14]P. Wagner, M.Sc. Thesis, Technical University of Berlin, 2009.
[15]N. N. Syrbu, M. Bogdanas, V. E. Tezlevan, and I. Mushcutariu, Physica B **229**, 199 (1997).
[16]For recent combined works of experiment and theory verifying the validity of a harmonic model potential, see, e.g., M. C. Rogge, E. Räsänen, and R. J. Haug, Phys. Rev. Lett. **105**, 046802 (2010).
[17]For a review, see S. M. Reimann and M. Manninen, Rev. Mod. Phys. **74**, 1283 (2002).
[18]A. Castro, H. Appel, M. Oliveira, C. A. Rozzi, X. Andrade, F. Lorenzen, M. A. L. Marques, E. K. U. Gross, and A. Rubio, Phys. Status Solidi B **243**, 2465 (2006).